



Behaviour of ozone in the hybrid ozonation-coagulation (HOC) process for ibuprofen removal: Reaction selectivity and effects on coagulant hydrolysis



Xin Jin^{a,b}, Shaohua Zhang^b, Shengjiong Yang^b, Yukai Zong^b, Lu Xu^a, Pengkang Jin^{a,b,*}, Chao Yang^b, Shiyi Hu^b, Yao Li^b, Xuan Shi^a, Xiaochang C. Wang^b

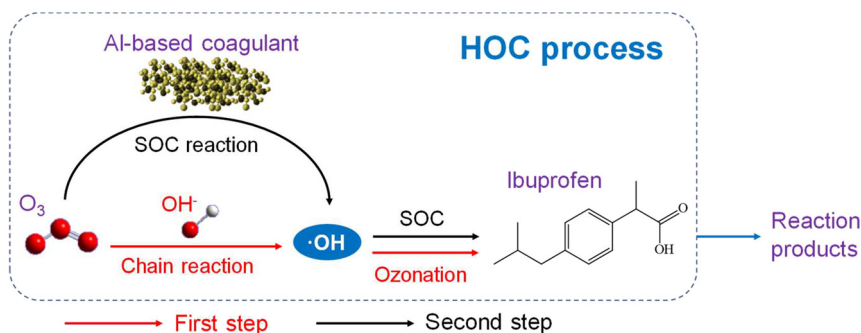
^a School of Human Settlements and Civil Engineering, Xi'an Jiaotong University, Xi'an, Shaanxi Province 710049, China

^b School of Environmental and Municipal Engineering, Xi'an University of Architecture and Technology, Xi'an, Shaanxi Province 710055, China

HIGHLIGHTS

- Higher IBP removal efficiency can be achieved from ozone dosage of 9.6 mg/L.
- Ozonation occurred prior to the reactions between ozone and coagulants in the HOC process.
- SOC effects could occur when the sufficient ozone was provided in the HOC process.
- Ozone can enhance the generation of polymeric species during the Al species hydrolysis.
- The generation of small molecular intermediates was promoted in the HOC process.

GRAPHICAL ABSTRACT



ARTICLE INFO

Article history:

Received 9 May 2021

Received in revised form 21 June 2021

Accepted 22 June 2021

Available online 24 June 2021

Editor: Huu Hao Ngo

Keywords:

Hybrid ozonation-coagulation process

Ibuprofen

Reaction selectivity

•OH generation

Hydrolysed species

ABSTRACT

Simultaneous ozonation and coagulation can be realized in one unit in the developed hybrid ozonation-coagulation (HOC) process. To reveal the reaction sequence within the HOC process, the ibuprofen (IBP) removal efficiency of the ozonation only, HOC and HOC- PO_4^{3-} (inhibition of the reactions between ozone and metal coagulant) processes at pH 5 and different ozone dosages were investigated. The removal efficiency is almost the same for the three processes at a low ozone dosage (4.8 mg/L), and higher removal performance can be achieved by the HOC process with increasing ozone dosage. It can be implied that ozone preferentially reacts with OH^- to generate $\bullet\text{OH}$ which react with IBP in the HOC process, and subsequently reacts with the surface hydroxyl groups of hydrolysed Al species to enhance $\bullet\text{OH}$ generation. Moreover, based on the kinetics, X-ray photoelectron spectroscopy (XPS) and Fourier transform infrared spectroscopy (FT-IR) analyses, the synergistic reactions between ozone and the metal coagulants (SOC) started to take effect from ozone dosage of 9.6 mg/L, which further verified that ozone will be involved in the IBP ozonation prior to the SOC reactions. The subsequent SOC reactions also resulted in the increased generation of polymeric Al species and more abundant intermediates in the HOC process.

© 2021 Elsevier B.V. All rights reserved.

* Corresponding author at: No. 28, Xianning West Road, Beilin district, Xi'an, China.

E-mail address: pkjin@hotmail.com (P. Jin).

1. Introduction

Ozonation and catalytic ozonation processes are well-recognized processes in the enhanced removal of biological refractory compounds (Huber et al., 2003; Lee and von Gunten, 2010; B. Zhang et al., 2021). To further improve the removal performance of organic pollutants, •OH generation is intended to be promoted, which is a less selective oxidant and can rapidly oxidize most types of organic moieties at diffusion-controlled rates ($\sim 10^8\text{--}10^9\text{ M}^{-1}\text{ s}^{-1}$) (Meunier et al., 2006). Moreover, it is an effective approach to add catalysts to the conventional ozonation process for improving the organic matter removal efficiency due to the enhanced •OH formation (Nawrocki, 2013; Nawrocki and Kasprzyk-Hordern, 2010).

Our previous work indicated that Al-based coagulants can also enhance •OH generation during ozonation (Jin et al., 2017; Jin et al., 2019a; Jin et al., 2019b). Consequently, the hybrid ozonation-coagulation (HOC) process was proposed, in which ozonation and coagulation occur simultaneously within a single unit (Jin et al., 2017). Similar to conventional heterogeneous catalytic ozonation, reactive oxygen species (ROS) can be generated through reactions between ozone and the surface groups of hydrolysed coagulant species, which are regarded as synergistic effects between ozone and metal coagulants (SOC) (Jin et al., 2020b). Nevertheless, for organic matter removal pathways within the HOC process, in addition to SOC effects, conventional ozonation can also occur, in which organic matters can be reacted through directly and indirectly ways. Therefore, conventional ozonation and SOC effects coexist in the HOC process. However, the behaviour of conventional ozonation and SOC effects within the HOC process for the reaction selectivity towards organic matters is still unclear.

In the HOC process, the in situ hydrolysis of added metal coagulant will proceed automatically as a result of the typical aqueous chemical equilibrium (Tang et al., 2015). For monomeric hydrolysis, in the cases of Al^{3+} and Fe^{3+} , it is known that the primary hydration shell can be formed, which consists of six water molecules in an octahedral coordination (Duan and Gregory, 2003). In addition, deprotonation can occur for the water molecules in the primary hydration shell to form hydroxyl groups, and hydrolysis can further proceed with the enhanced deprotonation effect (Duan and Gregory, 2003). At the same time, the polymerization process also occurred to form polynuclear species through hydroxyl bridges (Rustad and Casey, 2006; Yu et al., 2016), which led to an increase in net charge of the polycations during polymerization (Tang et al., 2015). Due to further hydroxylation, the precipitation will finally happen (Xiao et al., 2008; Yan et al., 2008; H. Zhao et al., 2009). Thereafter, many hydrolysed species can be generated via hydrolysis to form a series of products ranging from monomers, oligomers to polymeric hydroxyl complexes, including $\text{Al}(\text{OH})_2^{2+}$, $\text{Al}_2(\text{OH})_4^{4+}$, $\text{Al}(\text{OH})_4^-$, $\text{Al}_3(\text{OH})_5^{3+}$, $\text{AlO}_4\text{Al}_{12}(\text{OH})_{24}(\text{H}_2\text{O})_{12}^{7+}$ (Keggin- Al_{13} , also called Al_{13}) and $\text{Al}(\text{OH})_3$ (Shu-xuan et al., 2014; Xu et al., 2011). However, it was reported that ozone could react with the surface hydroxyl groups of hydrolysed coagulant species to generate ROS in the HOC process (Jin et al., 2017; Jin et al., 2019a; Jin et al., 2019b). Because of the deprotonation and hydroxyl bridging during the metal coagulant hydrolysis, the metal coagulant hydrolysed species formation within the HOC process can be affected through the reactions between ozone and surface hydroxyl groups. Nevertheless, there is little evidence about the effect of ozonation on metal coagulant hydrolysed species generation.

For the HOC process, conventional ozonation and •OH oxidation due to reactions between ozone and hydrolysed metal coagulants occurred simultaneously in one reactor. During conventional ozonation, •OH generation is limited compared with catalytic ozonation, and molecular ozone oxidation is the primary reaction, which exhibits low treatment efficiency for ozone-refractory pollutants (Nawrocki and Kasprzyk-Hordern, 2010; Wang and Chen, 2020). Nevertheless, •OH formation can be enhanced through the SOC effects in the HOC process, which can assist in eliminating ozone-refractory pollutants (Jin et al., 2017; Jin et al., 2019b; Jin et al., 2020b). There are three types of reactions for •OH oxidation, which include addition reactions, hydrogen-abstraction reactions and electron

transfer reactions, and the most common and fastest reactions are addition reactions (von Sonntag and von Gunten, 2012). Due to the different reaction mechanisms of conventional ozonation and •OH oxidation, different organic matter transformation intermediates or removal pathways can be expected. Sun et al. (2021) reported that •OH and ozone molecules reacted with different reaction sites of eugenol and generated different intermediates during •OH and ozone molecule oxidation (Fig. S1). It was also proposed that benzotriazole (BZA) exhibited different degradation pathways for conventional ozonation and •OH oxidation in the LaCoO_3 (LCO) catalytic ozonation process, and different intermediates were detected in the different degradation pathways (Zhang et al., 2020). For ibuprofen (IBP) decomposition, reaction pathways in E-peroxone treatment were proposed, in which the critical reaction steps for total mineralization were discussed (Li et al., 2014). Nevertheless, detailed reaction pathways of pollutants still need to be explored regarding the ozonation and catalytic ozonation procedure in the HOC process, which is important for further illustration of the reaction mechanism within the HOC process.

In this study, IBP was selected as the target pollutant, which is a typical personal care product, and frequently detected in WWTP effluents and surface waters. The IBP removal efficiency for the HOC process was investigated, and the quantitative contribution of different reactions within the HOC process was evaluated based on kinetics at different ozone dosages. The reaction selectivity between conventional ozonation and the SOC effects towards IBP within the HOC process is revealed according to the quantitative contribution evaluation, •OH generation detection, FT-IR, XPS analysis and degradation intermediate identification. In addition, the variation of coagulant hydrolysis in the HOC process was also investigated, and the effect of ozone on the hydrolysed Al species transformation was elucidated. The results provided mechanistic insights into the reactions within the HOC process for IBP removal.

2. Materials and methods

2.1. Reagents and chemicals

Ibuprofen (IBP), isopropanol (IPA), catalase (CAT), $(\text{CH}_3)_4\text{NOH}_5\cdot\text{H}_2\text{O}$ (TMA), 5,5-dimethyl-pyrroline-oxide (DMPO) were GR grade and purchased from Sigma-Aldrich. Acetonitrile was HPLC grade and purchased from Sigma-Aldrich. $\text{AlCl}_3\cdot 6\text{H}_2\text{O}$, HCl, H_3PO_4 , HNO_3 , H_2SO_4 , NaOH, Na_2HPO_4 , NaH_2PO_4 , Na_2SO_3 , $\text{Na}_2\text{S}_2\text{O}_3$, Na_2HPO_4 , and tert-butanol (TBA), KI, KBr, $\text{CH}_3\text{COONH}_4$, $\text{C}_5\text{H}_8\text{O}_2$ were analytical grade and obtained from Kermel, China. All the chemicals were used without further purification. The ultrapure water from a Millipore ultrapure water system (Milli-Q Elix-3) was used throughout the whole experiment process.

2.2. Ozonation, coagulation, and HOC experiments

The ozonation, coagulation and HOC experiments were conducted based on previous studies with some modifications (Jin et al., 2020a; Jin et al., 2019a; Jin et al., 2019b). In each experiment, 100 mL of IBP aqueous solution (50 μM) was used as the target contaminant of the reaction system. 0.2 mM phosphate buffer was added to the reaction system to ensure the pH stability. The pH value of the solution was adjusted to 5 using 0.1 M HCl or 0.1 M NaOH, and the coagulant $\text{AlCl}_3\cdot 6\text{H}_2\text{O}$ was added to achieve a dosage of 15 mg Al/L. 0.025 M Na_2SO_3 and $\text{Na}_2\text{S}_2\text{O}_3$ were added to samples to quench any residual ozone and hydroxyl radicals. The detailed ozonation, coagulation and HOC experiments conditions can be seen in Text S1.

2.3. Analytical methods

2.3.1. IBP analysis

For IBP analysis, the samples were collected from the reaction systems at pre-set time intervals. The concentration of IBP was quantified with high-performance liquid chromatography (HPLC) system (Shimadzu LC-2010AHF) attached with a UV detector and C18 column (5 μm particle

size, Global Chromatography, China). A mixture of water (adjusted to pH 2 with phosphoric acid) and acetonitrile in a volume ratio of 30:70 was used as the mobile phase. The detector was operated at 220 nm. The flow rate was kept at 1.0 mL/min and the injection volume was 10 μ L.

2.3.2. Fourier transform infrared spectroscopy (FT-IR) analysis

The samples were obtained by mixing the freeze-dried flocs and KBr with mass ratio of 1:49. An FT-IR spectrometer (Nicolet 6700, Thermo Fisher Scientific) was applied to analyse the samples with the range from 3950 to 450 cm^{-1} .

2.3.3. X-ray photoelectron spectra (XPS) analysis

A K-Alpha X-ray photoelectron spectrometer (Thermo Fisher Scientific, UK) was used to acquire the X-ray photoelectron spectra of Al 2p and O 1s peaks with the binding energy in the range from 100 to 1000 eV. The XPS data were analysed by using XPS peak fitting program XPSPEAK version 4.1.

2.3.4. •OH detection

The electron paramagnetic resonance (EPR) signal of •OH was detected using a Bruker EMX micro spectrometer (Germany) at room temperature. 200 mM 5,5-dimethyl-1-pyrroline N-oxide (DMPO) was added to the reaction system. The settings were center field 3500 G, sweep width 200 G, sweep time 40 s, receiver gain 30 dB, attenuation 60 dB, power 0.0002 mW, modulation frequency 100 kHz, conversion time 40 ms and time constant 20.48 ms.

The concentration of •OH in the solution was quantified by the tertiary butanol (t-BuOH) assay. •OH is scavenged by its reaction with t-BuOH (1.6 mM), which ultimately leads to formaldehyde formation. Formaldehyde was determined by the Hantzsch method (Nash, 1953).

2.3.5. Hydrolysed Al species analysis

The collected filtered samples were analysed using electrospray ionization/mass spectroscopy (ESI-MS) to identify the hydrolysed Al species (H. Zhao et al., 2009, 2011). ESI-MS spectra were recorded with a liquid chromatography tandem-mass spectrometry (LC-MS/MS, Waters Xevo TQD), and an electrospray ionization source (ESI) was operated in positive ion mode. Sample solutions were adjusted to pH 5 by 0.1 M tetramethylammonium hydroxide pentahydrate [(CH₃)₄NOH·5H₂O (TMA)] or HCl solution. The operating conditions were as follows: 5 μ L/min syringe pump flow rate, 3500 V capillary voltage, 30 V sample cone voltage, 5 V extraction cone voltage, 150 °C source temperature, 600 L/h cone gas flow rate, and 600 L/h desolvation gas flow rate.

2.3.6. Intermediate product analysis

The collected filtered samples were analysed using liquid chromatography-mass spectrometry (LC-MS) to identify the degradation intermediates of IBP. Details of the sample pre-treatment and LC-MS experimental conditions are described in Text S2, and the gradient elution conditions are shown in Table S1 in the supplementary material.

3. Results and discussion

3.1. Removal performance and quantitative evaluation

3.1.1. Removal performance of the HOC process

Fig. 1 shows the IBP removal efficiencies of the ozonation alone, HOC and HOC-PO₄³⁻ processes at pH 5 at the different ozone dosages (4.8, 9.6, 16.8, 24, 38.4 and 57.6 mg/L). According to Fig. 1, the IBP removal efficiency increased with increasing ozone dosage for all three different processes. Fig. 1 shows that approximately 90% IBP can be removed within 10 min for ozonation alone at ozone dosages 38.4 and 57.6 mg/L. Due to the low reaction rate constant with O₃ ($k_{\text{IBP, O}_3} = 9.1 \text{ M}^{-1} \text{ s}^{-1}$), IBP removal was primarily attributed to •OH oxidation ($k_{\text{IBP, •OH}} = 7.4 \times 10^9 \text{ M}^{-1} \text{ s}^{-1}$) (Huber et al., 2003). Furthermore, based on Fig. 1, higher IBP

removal efficiency can be obtained for the HOC process than that for the ozonation and HOC-PO₄³⁻ processes from ozone dosage of 9.6 mg/L. Because coagulation exhibited little IBP removal efficiency (Jin et al., 2020a), the higher IBP removal performance can be ascribed to enhanced •OH formation in the HOC process.

Nevertheless, the removal efficiency is exactly the same for the ozonation alone, HOC and HOC-PO₄³⁻ processes at a 4.8 mg/L ozone dosage. According to our previous studies, enhanced •OH generation was obtained through the reactions between ozone and hydrolysed metal coagulants in the HOC process (Jin et al., 2017; Jin et al., 2020a; Jin et al., 2019a; Jin et al., 2019b). Therefore, at a low ozone dosage (4.8 mg/L), it can be implied that the SOC effects, i.e., the reactions between ozone and hydrolysed metal coagulants barely occurred. Because the added PO₄³⁻ can bind with the surface hydroxyl groups of the hydrolysed metal coagulants (Ren et al., 2012; Zhao et al., 2015), the reactions between ozone and hydrolysed metal coagulants can be inhibited in the HOC process. As a consequence, the almost same removal performances of the HOC-PO₄³⁻ and HOC processes further indicated that only conventional ozonation happened in the HOC process at low ozone dosage. In other words, higher IBP removal efficiency could have been observed at ozone dosage of 4.8 mg/L for the HOC process if ozone preferentially reacted with metal coagulants to generate more •OH. Therefore, it was possible that ozone firstly reacted with OH⁻ to generate •OH for the IBP decomposition rather than that with coagulants. However, with the increasing ozone dosage (from an ozone dosage of 9.6 mg/L), ozone started to react with coagulants to produce •OH, increasing the removal efficiency of the HOC process. It can be acquired that the SOC effects started to work when there was enough ozone in the HOC system based on the comparison between removal performance at ozone dosage of 4.8 mg/L and 9.6 mg/L. Furthermore, the advantages of the HOC process became more and more obvious with the increasing ozone dosages according to Fig. 1. In consequence, it can be inferred that IBP first was reacted during conventional ozonation in the HOC process and was subsequently oxidized by the •OH generated from the SOC effects in the HOC process.

In addition, TOC removal performance of IBP for the three different processes was also obtained at different ozone dosages at pH 5 (Fig. S2). According to Fig. S2, the TOC removal efficiency of IBP was exactly the same for the ozonation alone, HOC and HOC-PO₄³⁻ processes at ozone dosage of 4.8 mg/L. However, higher TOC removal efficiency can be obtained for the HOC process than that for the ozonation and HOC-PO₄³⁻ processes from ozone dosage of 9.6 mg/L. Therefore, it further indicated that only conventional ozonation happened in the HOC process at low ozone dosage (4.8 mg/L ozone dosage). With the increasing ozone dosage (from an ozone dosage of 9.6 mg/L), ozone started to react with coagulants to produce more •OH, increasing the TOC removal efficiency of IBP. Furthermore, compared with the ozonation and HOC-PO₄³⁻ processes, approximately 80%–90% TOC removal efficiency of IBP can be obtained within 10 min for the HOC process at ozone dosages 38.4 and 57.6 mg/L. This further implied that the higher IBP mineralization performance can be ascribed to enhanced •OH formation in the HOC process due to the SOC effects.

3.1.2. Quantitative analysis of reactions within the HOC process

Based on our previous work, coagulation, direct molecular ozone oxidation (MO reactions), peroxone reactions (O₃/H₂O₂), and •OH oxidation due to reactions between O₃ and OH⁻ (HO reactions) and the synergistic reactions between ozone and metal coagulants (SOC) co-existed within the HOC processes (Jin et al., 2020b). To estimate the contribution to IBP removal for the different reactions quantitatively, a series of trapping experiments were conducted through the addition of excess •OH scavenger (isopropanol (IPA)) and H₂O₂ scavenger (catalase (CAT)) to the ozonation and HOC system with pH 5 at different ozone dosages (4.8, 9.6, 16.8, 24, 38.4 and 57.6 mg/L) (Jin et al., 2020b; Xiong et al., 2018). The pseudo-first-order rate constant (k_{obs}) of each reaction within the HOC process can be calculated based on the trapping experiments (Jin et al., 2020b; Liu et al., 2014; Mu et al., 2017; Wang et al., 2020; Xiong et al., 2018),

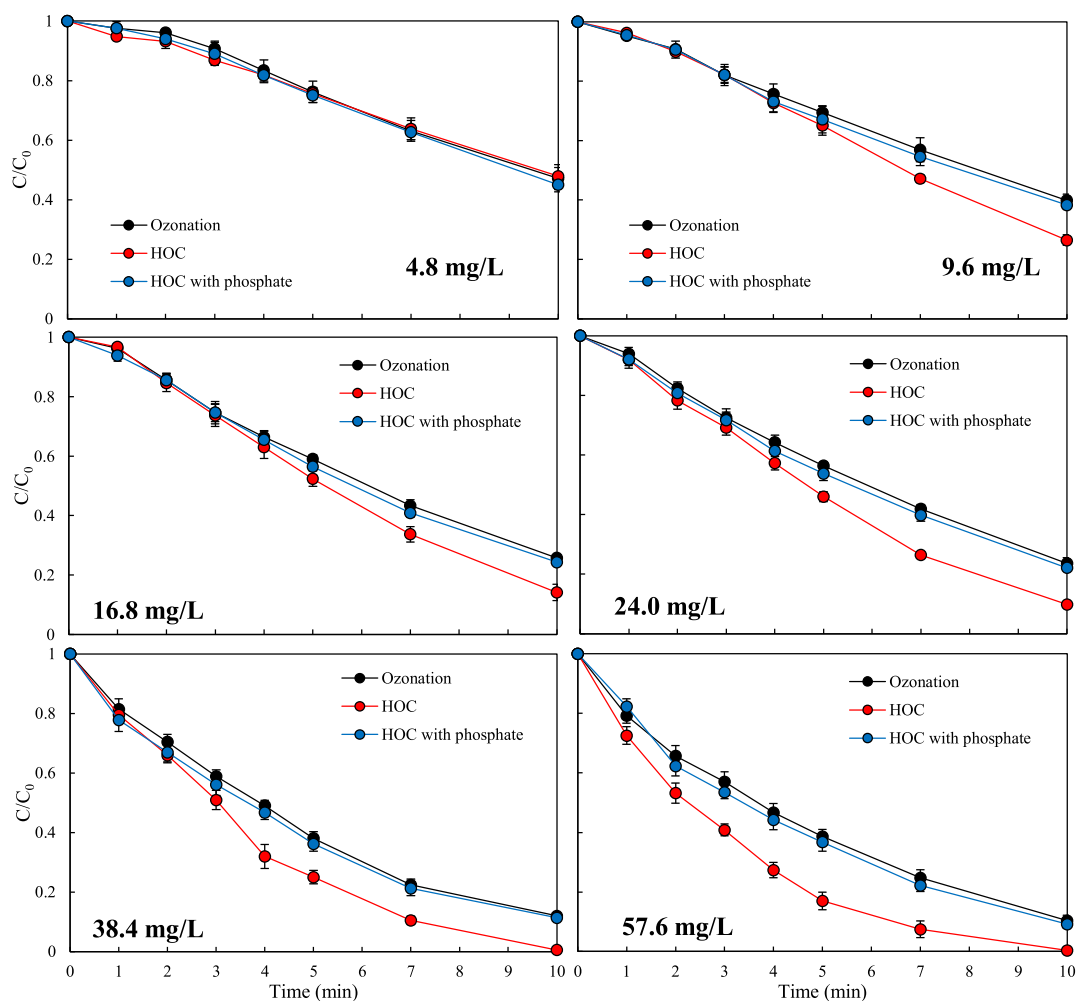


Fig. 1. Comparison between the ozonation alone, HOC and HOC- PO_4^{3-} process for IBP removal at pH 5 at different ozone dosages.

and the k_{obs} values of each reaction can be seen in Table S2. The calculation method of the relative contribution of involved reactions within the HOC process can be seen in Table S3. The IBP removal performance achieved with the addition of different scavengers can be seen in Fig. S3, and the kinetics analysis of the experiments with the addition of different scavengers is shown in Fig. S4.

In addition, $\bullet\text{O}_2^-$ and 1O_2 trapping experiments for the HOC process were also conducted to test the contribution of $\bullet\text{O}_2^-$ and 1O_2 oxidation by using p-benzoquinone (BQ, $\bullet\text{O}_2^-$ scavenger) (Y. Zhang et al., 2021) and sodium azide (NaN_3 , 1O_2 scavenger) (Jawad et al., 2014) based on the addition of IPA to inhibit the $\bullet\text{OH}$ oxidation, i.e. HOC + IPA + BQ or HOC + IPA + NaN_3 . The results can be seen in Fig. S5. If $\bullet\text{O}_2^-$ or 1O_2 oxidation are responsible for IBP removal in the HOC process, the IBP removal efficiency should be further inhibited after the addition of BQ or NaN_3 . However, the IBP removal efficiency were almost the same compared with the addition of IPA alone i.e. HOC + IPA (Fig. S5). Therefore, it can be inferred that the contribution of $\bullet\text{O}_2^-$ and 1O_2 exhibited little effect on IBP removal in the HOC process.

The contribution of coagulation within the HOC process can be acquired according to the calculated proportion of the k_{obs} of coagulation alone to that of the HOC process (Table S2). The results indicated that the contributions of coagulation to IBP removal within the HOC process were 3.40%, 1.88%, 1.27%, 1.08%, 0.52% and 0.48% at ozone dosages of 4.8, 9.6, 16.8, 24, 38.4 and 57.6 mg/L, respectively (Fig. 2), which remained almost constant for different ozone dosages. This can be attributed to the low IBP removal ability of coagulation. Moreover, the contribution of direct molecular ozone oxidation (MO reactions) can be calculated

according to Table S3, and the results were 44.70%, 32.13%, 25.84%, 25.69%, 18.64% and 22.03% at ozone dosages of 4.8, 9.6, 16.8, 24, 38.4 and 57.6 mg/L, respectively (Fig. 2). Obviously, the contribution of MO reactions decreased to a constant value (~20%) as the ozone dosage increased. These phenomena resulted from enhanced $\bullet\text{OH}$ generation due to the increased ozone dosages.

In this study, H_2O_2 can be produced in the HOC process through Eqs. (1)–(3) (Xiong et al., 2018; Zhang et al., 2011), hence peroxide reactions existed within the HOC process (Eqs. (4)–(5)) (Jin et al., 2020a). The contribution of peroxide reactions can be calculated according to the k_{obs} of the H_2O_2 trapping experiments (HOC + CAT) (Table S2). As shown in Fig. 2, the contributions of the peroxide reactions can be obtained, i.e., 17.93%, 24.55%, 31.60%, 27.72%, 26.86% and 14.18% corresponding to ozone dosages of 4.8, 9.6, 16.8, 24, 38.4 and 57.6 mg/L, respectively (Fig. 2).



Furthermore, the contribution of HO reactions in the HOC process can be acquired according to Table S3, and the results were 33.56%,

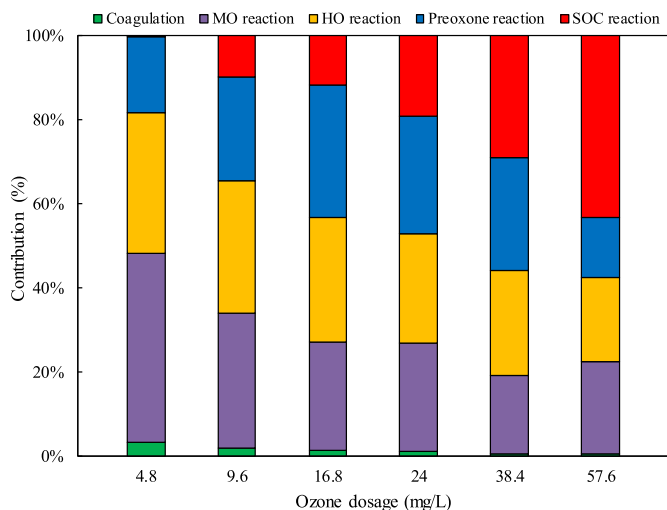


Fig. 2. Contributions of different reactions in the HOC process at pH 5 with different ozone dosages.

31.46%, 29.61%, 26.21%, 24.98% and 20.07% at ozone dosages of 4.8, 9.6, 16.8, 24, 38.4 and 57.6 mg/L, respectively (Fig. 2). It was revealed that the contribution of HO reactions remained relatively stable in the HOC process. Previous studies have shown that pH can affect the ozone decomposition, and hydroxide ions (OH^-) of the solution can initiate the decomposition of O_3 into $\bullet\text{OH}$ by the chain reactions (Eqs. (6)–(9)) (Staelin and Hoigne, 1982). The contribution of HO reactions remained almost constant at different ozone dosages because the pH was controlled and stable at pH 5 in the HOC process.



Finally, after the deduction of the k_{obs} of all the above reactions from the HOC process, the contribution of the SOC reactions between ozone and the hydrolysed aluminium species can be obtained (Table S2) as 0.41%, 9.98%, 11.67%, 19.30%, 29.00% and 43.24% at ozone dosages of 4.8, 9.6, 16.8, 24, 38.4 and 57.6 mg/L, respectively (Fig. 2). The contribution of the SOC reactions gradually increased with increasing ozone dosage, which illustrated that the reactions between ozone and hydrolysed metal coagulants did not occur at low ozone dosages, and ozonation was mainly responsible for the initial IBP removal for the HOC process. Moreover, the SOC reactions took effect from the ozone dosage of 9.6 mg/L, which enhanced the $\bullet\text{OH}$ generation.

3.2. Reaction selectivity analysis

3.2.1. FT-IR analysis

FT-IR was used to characterize the properties of the hydrolysed Al species generated from $\text{AlCl}_3 \cdot 6\text{H}_2\text{O}$ at pH 5 with different ozone dosages (4.8, 9.6, 16.8, 24, 38.4 and 57.6 mg/L) to further explore the SOC reactions within the HOC process. According to previous studies, the peaks at approximately 3450 cm^{-1} and 1640 cm^{-1} were attributed to the vibration mode of chemically bonded surface hydroxyl groups and the deformation vibration of water molecules attached to the surface of the hydrolysed metal coagulants, respectively (Huang et al., 2019; Jin et al., 2020a; Jin et al., 2019b; Li et al., 2004). As depicted in Fig. 3, significant peak intensity decrease for the hydroxyl groups on the surface of the hydrolysed Al species in the ultrapure water system for the HOC

process at different ozone dosages can be observed. This phenomenon indicated that the surface hydroxyl groups served as the active sites to react with ozone (Magureanu et al., 2011; Wang et al., 2016). It was reported that Al-bonded hydroxyl group (Al-OH) was a type of strong Lewis acid sites (Bing et al., 2015; Wang et al., 2018; Yang et al., 2009). As a dipole molecule, one oxygen atom of an ozone molecule, which acts as Lewis base, can be chemically adsorbed onto Al-OH to further generate reactive oxygen species within the HOC process. However, the intensity of the peak at 3450 cm^{-1} representing the surface hydroxyl groups exhibited little variation at a 4.8 mg/L ozone dosage in the HOC process in the presence of IBP (Fig. 3). This further implied that ozone was consumed during ozonation for the reaction of IBP, and hardly any reactions between the surface hydroxyl groups of hydrolysed Al species and ozone could be observed. When the ozone dosage was higher than 9.6 mg/L, the peak intensity began to decrease but was still higher than that of the ultrapure water system. Hence, ozonation preferentially occurred in the HOC process at low dosages, and subsequently, the SOC effects occurred to improve $\bullet\text{OH}$ formation within the HOC process.

3.2.2. XPS analysis

Figs. S6, S7 and S8 show the Al 2p XPS spectra of $\text{AlCl}_3 \cdot 6\text{H}_2\text{O}$ for the coagulation and HOC processes at pH 5 with the different ozone dosages (4.8, 9.6, 16.8, 24, 38.4 and 57.6 mg/L). Two overlapping bands related to two different Al 2p peaks were found (Fig. S6), which can be assigned to the tetrahedral Al (binding energy 73.1 eV) and octahedral Al (binding energy 74.2 eV) signals (Duong et al., 2005; Lin et al., 2014). As the ozone dosage increased, there is a decrease in the proportion of tetrahedral Al in the HOC process compared with that of the coagulation process (Fig. S9). A previous study reported that it was stronger Lewis acid site for surface tetrahedral Al than that for the surface octahedral Al (Flura et al., 2012). Therefore, it was more favourable for ozone to react with tetrahedral Al to decompose molecular ozone into ROS. However, in contrast to the ultrapure water system, the ratio of tetrahedral Al was almost the same for the coagulation and HOC processes with IBP at a low ozone dosage (4.8 mg/L). This result indicated that ozone will first be involved in the IBP ozonation and then start to react with tetrahedral Al species to enhance the ROS generation.

In addition, Figs. S10, S11 and S12 represent the O 1s XPS spectra of $\text{AlCl}_3 \cdot 6\text{H}_2\text{O}$, whose peaks can be assigned to lattice oxygen (O_α), surface hydroxyl groups (O_β) and adsorbed water (O_γ) with binding energy 530.7 eV, 531.5 eV and 532.4 eV, respectively (Ding et al., 2016). It was observed that the ratio of O_β was almost the same for the coagulation and HOC processes with IBP at a low ozone dosage (4.8 mg/L) and dropped compared with that of the coagulation process from ozone dosage of 9.6 mg/L (Fig. S13). The results verified again that ozone will first be involved in the IBP ozonation and that the interactions between ozone and surface hydroxyl groups of the hydrolysed Al species will happen next.

3.2.3. $\bullet\text{OH}$ generation

EPR tests with DMPO as the spin trapping agent were performed to further verify $\bullet\text{OH}$ formation within the HOC process. The results can be seen in Fig. 4. At a low ozone dosage (4.8 mg/L), a low peak intensity can be detected for the ozonation alone, HOC and HOC- PO_4^{3-} processes, and little difference can be observed between the three different processes. With the increasing ozone dosages, the peak intensity detected in the HOC process became stronger than that detected in the other two processes. In addition, the overlapping spectra were composed of three different signals that represented DMPO- $\bullet\text{OH}$ adducts (marked with the cycle symbols), carbon-centred radical adducts (marked with arrow symbols) and oxidized DMPO radicals (marked with rectangle symbols), respectively. The presence of DMPO- $\bullet\text{OH}$ adducts provides additional evidence of $\bullet\text{OH}$ generation within the HOC process, and enhanced $\bullet\text{OH}$ formation was also observed after the ozonation of IBP. Moreover, DMPO can also be oxidized in the three processes to feature

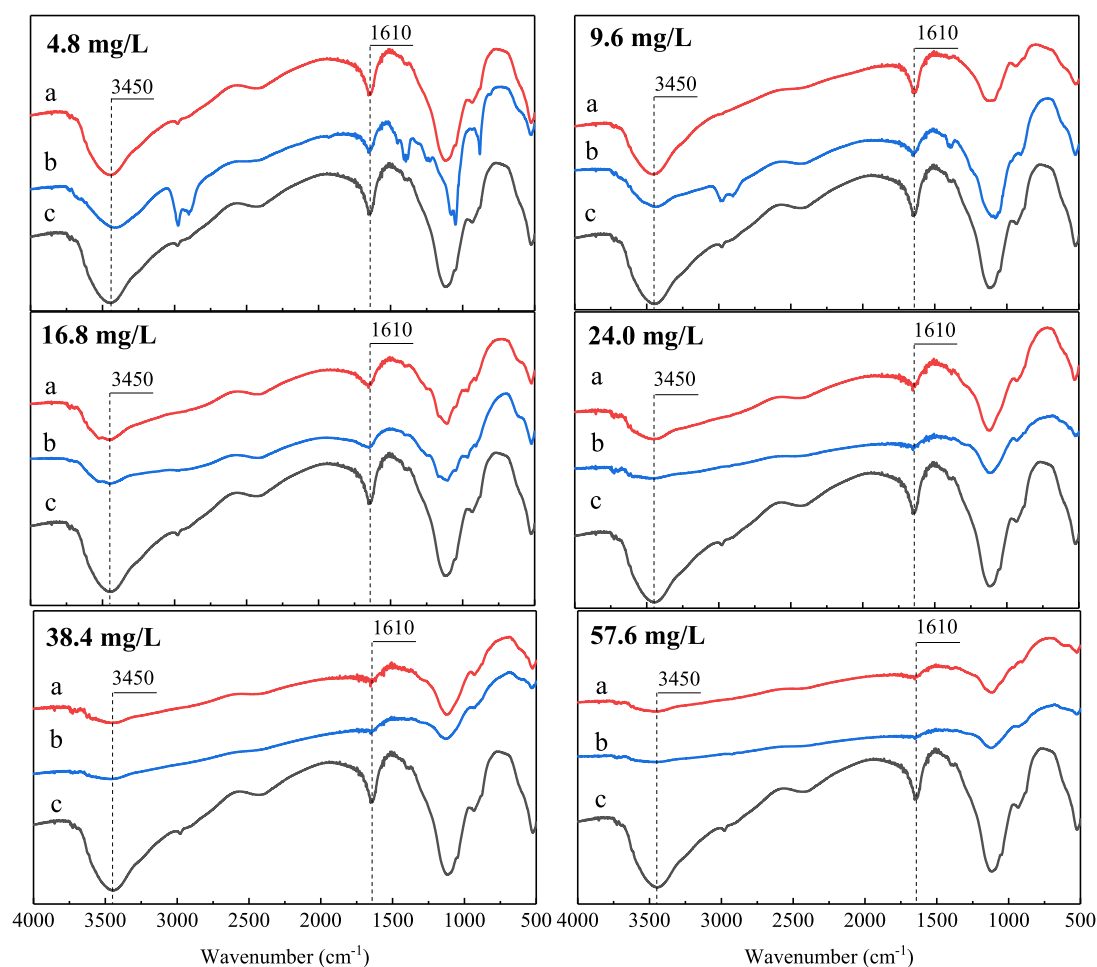


Fig. 3. FT-IR spectra in the HOC process with IBP (a), HOC process in ultrapure water (b) and coagulation process (c) at pH 5 at different ozone dosages.

a three-line spectrum (Feng et al., 2016). It was also reported that the attack of carbon containing compounds by $\bullet\text{OH}$ could result in the appearance of carbon-centered radicals adduct with a six-peak spectrum (Dong et al., 2014; Khachatryan and Dellinger, 2011; Wang et al., 2013), which further proved the oxidation of IBP by $\bullet\text{OH}$ within the HOC process. Moreover, the absence of six-peak spectrum in the

ultrapure water system verified the existence of carbon-centred radicals within the HOC process with IBP (Fig. S14).

For the three different processes (ozonation, HOC and HOC-PO_4^{3-} processes), the generation of $\bullet\text{OH}$ was quantified by the t-BuOH assay (Nöthe et al., 2009). The results can be seen in Fig. 5. The $\bullet\text{OH}$ generation was much higher in the ultrapure water system than that of IBP system,

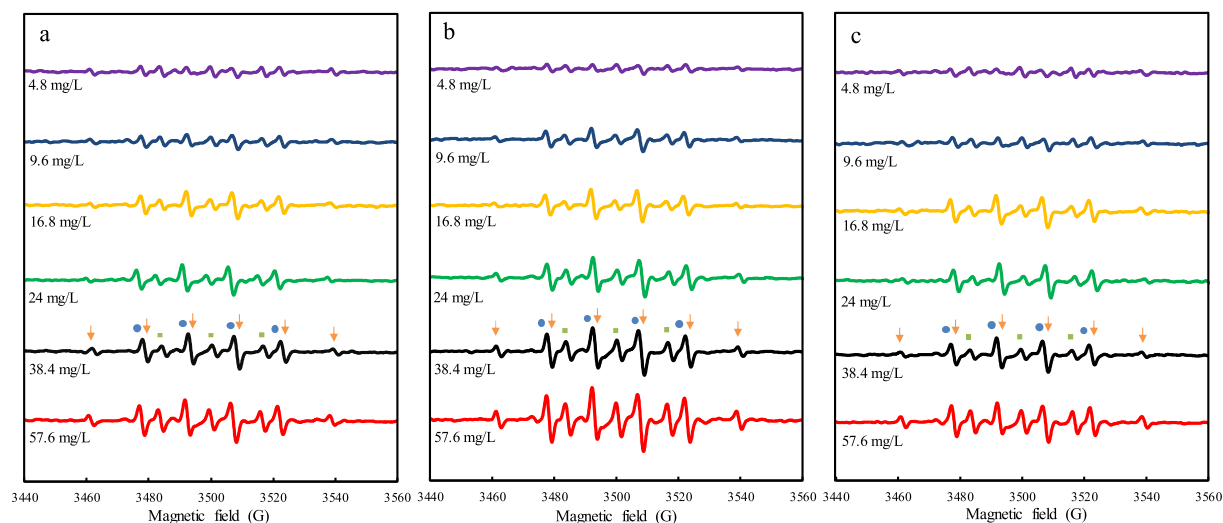


Fig. 4. EPR spectra in the ozonation alone (a), HOC (b) and HOC-PO_4^{3-} (c) process for IBP removal at pH 5 at different ozone dosages.

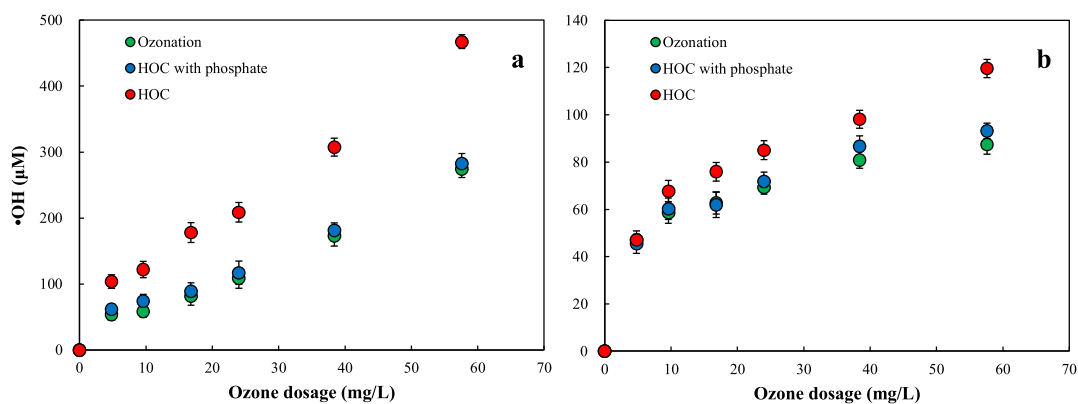


Fig. 5. •OH generation at different ozone dosages. (a) ultrapure water system; (b) IBP system.

which can be attributed to •OH consumption during IBP oxidation (Hama Aziz et al., 2017; Saeid et al., 2018). In addition, the HOC process can produce more •OH than other two processes in both the ultrapure water and IBP systems, which proved the catalytic ability of hydrolysed Al species. However, different from that in the ultrapure water system, the •OH generation in the HOC process was not always higher than ozonation and HOC- PO_4^{3-} processes. The •OH generation was almost the same for the three processes at low ozone dosages. This result further indicated that ozone will first be involved in IBP ozonation and then start to react with hydrolysed Al species to enhance •OH generation, which results in the higher •OH concentration than other two processes. Little difference in •OH generation can be observed between the HOC- PO_4^{3-} and ozonation processes for both the ultrapure water and IBP systems, further verifying that the surface hydroxyl sites was the active sites for the reactions with ozone to generate •OH.

3.3. Hydrolysed Al species analysis

In order to further elucidate the mechanism within the HOC process, the effect of ozone on the distribution of hydrolysed Al species was analysed based on ESI-MS analysis. The ESI-MS spectra obtained at different ozone dosages for coagulation and the HOC process with and

without IBP are shown in Figs. S15, S16 and S17, respectively. According to the mass-to-charge ratio (m/z), aluminium species can be distinguished (Feng et al., 2011; Sarpola et al., 2004; H. Zhao et al., 2009, 2011). The signals of Al species detected in the ESI-MS spectra are shown in Table S4. Five aluminium species were categorized as follows: Al_1 - Al_2 species (monomeric and dimeric aluminium complexes), Al_3 - Al_5 species (small polymeric aluminium species), Al_6 - Al_{10} species (median polymeric species), Al_{11} - Al_{21} species (large polymeric species) and undetected species (Al_n , i.e., solid-phase $\text{Al}(\text{OH})_3$ and/or $\text{Al}(\text{OH})_4^-$) (H. Zhao et al., 2009). The abundance of polymeric Al species was estimated semi-quantitatively by the signal intensities of relative to Al species (Rämö et al., 2008). The results can be seen in Fig. 6. The proportions of polymeric Al species increased with the increasing ozone dosages for both the HOC with and without IBP, which indicated that the addition of ozone could facilitate polymerization during Al species hydrolysis in general. In addition, for the low ozone dosage (4.8 mg/L), the variation of Al species was smaller than that of higher ozone dosages (24 and 57.6 mg/L), which indicated that reactions between ozone and hydrolysed Al species were limited at low ozone dosages. Moreover, the addition of IBP retarded the polymerization process during the Al hydrolysis at the same ozone dosage (Fig. 6). This can be attributed to the preferential reactions between IBP and ozone. Therefore, due to

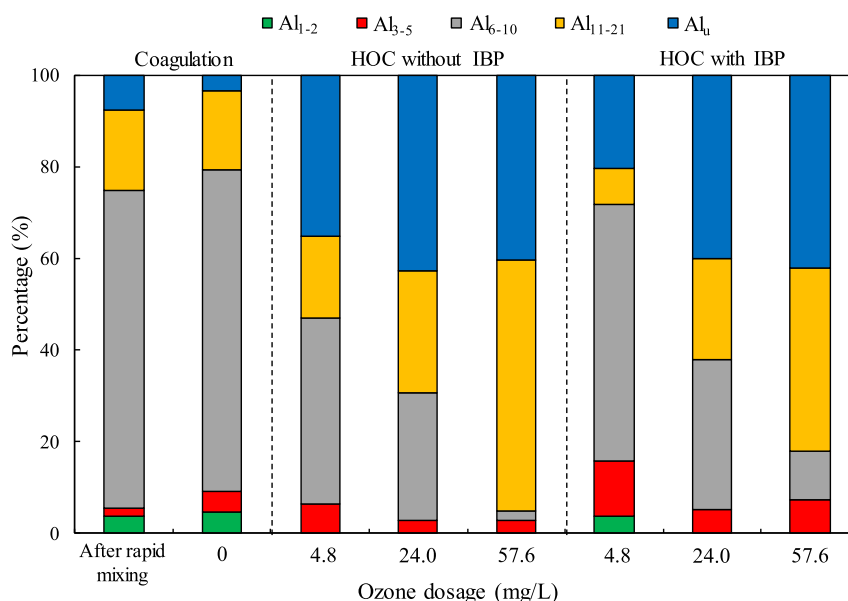


Fig. 6. Distribution of hydrolysed Al species in coagulation and the HOC process at pH 5.

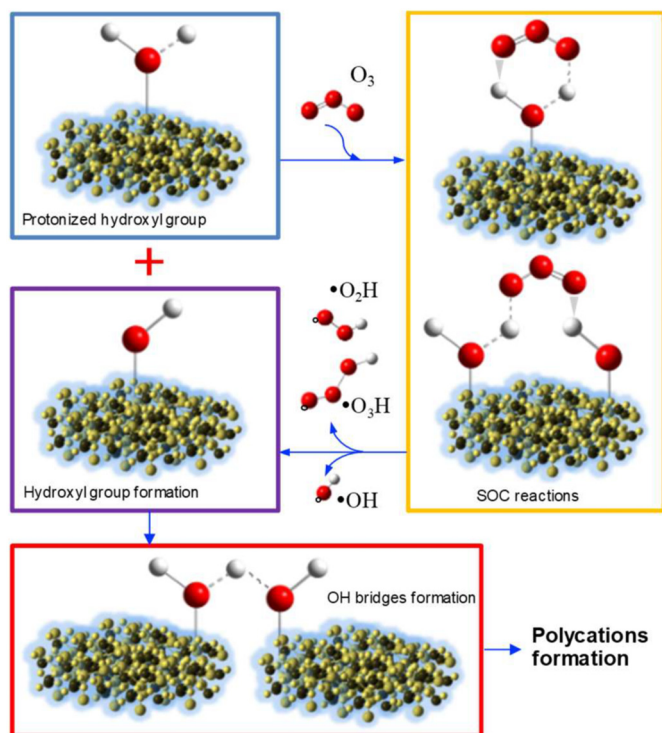
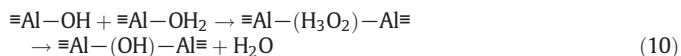


Fig. 7. Effect of ozone on the polymerization process of hydrolysed Al species.

immediate reactions between ozone and coagulant, the content of polymerized Al species within the HOC process without IBP was higher than that with IBP.

Due to the acidic condition of the aqueous solution ($\text{pH} = 5$ in this case), the surface protonated hydroxyl groups should be the predominant surface group. In addition, for ozone molecule, it has both an electrophilic and a nucleophilic site (Kasprzyk-Hordern et al., 2003; L. Zhao et al., 2009). It was reported that ozone in aqueous solution tends to interact with the surface protonated hydroxyl groups on the catalysts, which is driven by electrostatic forces and/or hydrogen bonding (L. Zhao et al., 2009). Thereafter, the interactions between ozone and surface protonated hydroxyl groups result in the release of $\bullet\text{O}_3\text{H}$, $\bullet\text{O}_2\text{H}$ and $\bullet\text{OH}$ to form surface hydroxyl groups. Subsequently, the generated surface —OH groups can bind with surface —OH_2 to form $\text{—OH}\cdot\text{OH}_2$ bridges (Rustad and Casey, 2006). After releasing H_2O , the OH bridges can finally form to achieve polymerization according to Eq. (10) (Yu et al., 2016). Therefore,

the presence of ozone can enhance the generation of polymeric species during Al species hydrolysis. Fig. 7 shows the effect of ozone on the polymerization process of hydrolysed Al species.



3.4. IBP intermediate product analysis

The IBP degradation intermediates of the ozonation, HOC- PO_4^{3-} and HOC processes were recognized by ultra-high phase liquid mass spectrometry (UHPLC-MS) between the m/z range 50–400 in negative ionization mode at ozone dosage of 24 mg/L. The molecular structure for each intermediate/product was proposed according to the molecular ion masses and MS fragmentation patterns. MS spectra for each intermediate/product can be seen in Fig. S18. The chemical structure and properties of IBP degradation products are shown in Table S5. In total, twenty intermediates were identified in this study for the three different treatment processes (ozonation alone, HOC and HOC- PO_4^{3-} processes) as shown in Fig. S18. In addition, there were three intermediates only detected in the HOC process, and the intermediates detected in the ozonation alone and HOC- PO_4^{3-} processes were the same.

According to the detected intermediates, the possible reaction pathways for IBP degradation by three different treatment processes can be seen in Fig. 8. Due to the same detected intermediates, the same reaction pathway can be proposed for the ozonation alone and HOC- PO_4^{3-} processes. Because of the very low reaction rate between molecular ozone and IBP ($k = 9.1 \text{ M}^{-1} \text{ s}^{-1}$) and high reaction rate between $\bullet\text{OH}$ and IBP (Huber et al., 2003), the transformation and removal of IBP can be mainly attributed to $\bullet\text{OH}$ oxidation (Li et al., 2014). Fig. 8 shows that the detected primary intermediates are the same for the three different processes via hydroxylation and decarboxylation of $\bullet\text{OH}$ attack, which further proved that the $\bullet\text{OH}$ oxidation of IBP through ozonation occurred initially rather than $\bullet\text{OH}$ oxidation through reactions between the hydrolysed coagulant and ozone within the HOC process. Based on previous studies (Rao et al., 2016; Ruggeri et al., 2013), it was more favourable for the hydroxylation on the side chains than that on the benzene ring. Therefore, three isomer compounds of monohydroxylated IBP (compound 2, 3 and 4) and a compound of multihydroxylated IBP (compound 5) can be found as the primary intermediates. In addition, the generation of 1-ethyl-4-isobutyl benzene (compound 6) was attributed to the decarboxylation of the propanoic acid chain of IBP (Rao et al., 2016).

Afterwards, the decarboxylated, demethylated and hydrogen abstracted products such as compounds 7–12 were formed due to $\bullet\text{OH}$ attack in the next step (Peng et al., 2020; Rubasinghege et al., 2018; Xiang

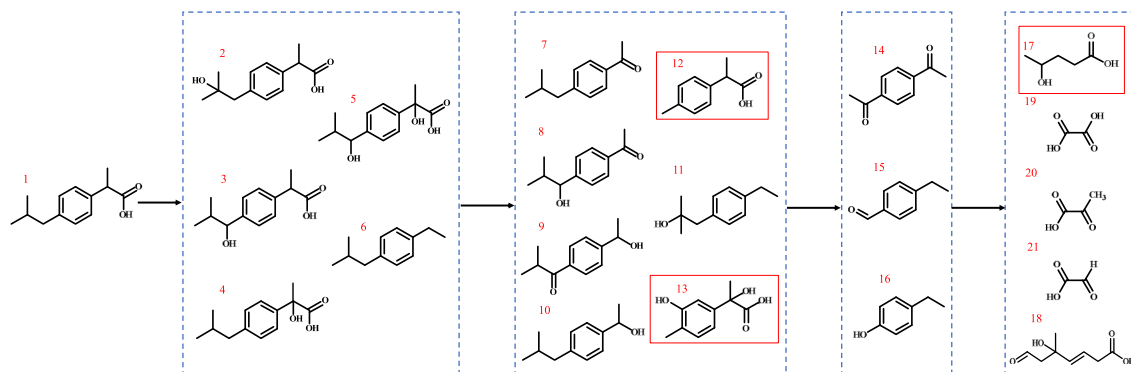


Fig. 8. Possible reaction pathways of IBP in the ozonation alone, HOC and HOC- PO_4^{3-} processes. The compounds with red rectangle represented the compounds only detected in the HOC process.

et al., 2016). Specifically, compounds 12 and 13 can only be detected within the HOC process due to enhanced $\bullet\text{OH}$ formation, which indicated that ozone started to react with hydrolysed coagulant species. 2-(p-tolyl)propanoic acid (compound 12) was generated from the demethylation of compound 2. Moreover, hydroxylation on the benzene ring due to the improved oxidation ability of the HOC process and demethylation of the side chains of compounds 4 and 5 can yield 2-hydroxy-2-(3-hydroxy-4-methylphenyl)propanoic acid (compound 13). Thereafter, smaller aromatic compounds such as compounds 14, 15 and 16 were yielded with further decarboxylation, demethylation and hydrogen abstraction (Li et al., 2014; Peng et al., 2020). The smaller aromatic compounds were likely cleaved by $\bullet\text{OH}$ producing a variety of carboxylic acids, and one more compound (compound 17, 5-hydroxyhexan-2-one) was detected during the HOC process (Li et al., 2014; Peng et al., 2020). The yielded carboxylic acids could eventually be oxidized to CO_2 and H_2O , accomplishing mineralization, which was also proved in Fig. S2. The three more detected smaller oxidized compounds during the HOC process further implied enhanced $\bullet\text{OH}$ generation due to the SOC effects after the first step of $\bullet\text{OH}$ oxidation during initial ozonation.

4. Conclusion

The removal efficiency is almost the same for the ozonation alone, HOC and HOC-PO_4^{3-} processes at ozone dosage of 4.8 mg/L. However, compared with the ozonation and HOC-PO_4^{3-} processes, a higher IBP removal efficiency can be obtained for the HOC process from ozone dosage of 9.6 mg/L. This indicated that IBP was first oxidized during ozonation in the HOC process, and subsequently further oxidized by $\bullet\text{OH}$ due to enhanced $\bullet\text{OH}$ generation in the SOC reaction. Moreover, based on the quantitative analysis of reactions within the HOC process, SOC reactions mainly occurred from ozone dosage of 9.6 mg/L. FT-IR and XPS analyses further proved that the reactions between ozone and the hydrolysed Al species happened mostly from ozone dosage of 9.6 mg/L. In addition, the SOC reactions can also improve the polymerization process during Al-based coagulant hydrolysis to increase polymeric Al species formation and promote small molecular intermediates generation in the HOC process.

CRediT authorship contribution statement

Xin Jin: Conceptualization, Methodology, Funding acquisition, Writing – original draft, Writing – review & editing. **Shaohua Zhang:** Investigation, Writing – original draft. **Shengjiang Yang:** Investigation, Validation. **Yukai Zong:** Investigation, Validation. **Lu Xu:** Methodology, Investigation. **Pengkang Jin:** Supervision, Funding acquisition, Writing – review & editing, Project administration. **Chao Yang:** Methodology. **Shiyi Hu:** Visualization. **Yao Li:** Validation. **Xuan Shi:** Visualization. **Xiaochang C. Wang:** Writing – review & editing.

Declaration of competing interest

The authors declare that they have no known competing financial interests or personal relationships that could have appeared to influence the work reported in this paper.

Acknowledgements

This work was supported by the National Key Research and Development Program of China (No. 2019YFB2103003), the National Natural Science Foundation of China (No. 52070151, 51708443), the Key Research and Development Project of Shaanxi Province (No. 2019ZDLSF05-03), Technology Innovation Leading Program of Shaanxi (No. 2020CGXNG-021), National College Students Innovation and Entrepreneurship Training Program (S202010703084) and the New Style Think Tank of Shaanxi Universities.

Appendix A. Supplementary data

Supplementary data to this article can be found online at <https://doi.org/10.1016/j.scitotenv.2021.148685>.

References

- Bing, J., Hu, C., Nie, Y., Yang, M., Qu, J., 2015. Mechanism of catalytic ozonation in $\text{Fe}_2\text{O}_3/\text{Al}_2\text{O}_3@ \text{SBA-15}$ aqueous suspension for destruction of ibuprofen. *Environ. Sci. Technol.* 49 (3), 1690–1697.
- Ding, Y., Zhou, P., Tang, H., 2016. Visible-light photocatalytic degradation of bisphenol A on NaBiO_3 nanosheets in a wide pH range: a synergistic effect between photocatalytic oxidation and chemical oxidation. *Chem. Eng. J.* 291, 149–160.
- Dong, G., Ai, Z., Zhang, L., 2014. Total aerobic destruction of azo contaminants with nano-scale zero-valent copper at neutral pH: promotion effect of in-situ generated carbon center radicals. *Water Res.* 66, 22–30.
- Duan, J., Gregory, J., 2003. Coagulation by hydrolysing metal salts. *Adv. Colloid Interf. Sci.* 100–102, 475–502.
- Duong, L.V., Wood, B.J., Klopogge, J.T., 2005. XPS study of basic aluminum sulphate and basic aluminum nitrate. *Mater. Lett.* 59 (14), 1932–1936.
- Feng, C., Zhao, S., Bi, Z., Wang, D., Tang, H., 2011. Speciation of prehydrolyzed Al salt coagulants with electrospray ionization time-of-flight mass spectrometry and ^{27}Al NMR spectroscopy. *Colloids Surf. A Physicochem. Eng. Asp.* 392 (1), 95–102.
- Feng, G., Cheng, P., Yan, W., Boronat, M., Li, X., Su, J.-H., Wang, J., Li, Y., Corma, A., Xu, R., Yu, J., 2016. Accelerated crystallization of zeolites via hydroxyl free radicals. *Science* 351 (6278), 1188.
- Flura, Aurélien, Can, Fabien, Courtois, Xavier, Royer, Sébastien, Duprez, D., 2012. High-surface-area zinc aluminate supported silver catalysts for low-temperature SCR of NO with ethanol. *Appl. Catal. B Environ.* 126 (38), 275–289.
- Hama Aziz, K.H., Miessner, H., Mueller, S., Kalass, D., Moeller, D., Khorshid, I., Rashid, M.A.M., 2017. Degradation of pharmaceutical diclofenac and ibuprofen in aqueous solution, a direct comparison of ozonation, photocatalysis, and non-thermal plasma. *Chem. Eng. J.* 313, 1033–1041.
- Huang, Y., Luo, M., Xu, Z., Zhang, D., Li, L., 2019. Catalytic ozonation of organic contaminants in petrochemical wastewater with iron-nickel foam as catalyst. *Sep. Purif. Technol.* 211, 269–278.
- Huber, M.M., Canonica, S., Park, G.-Y., von Gunten, U., 2003. Oxidation of pharmaceuticals during ozonation and advanced oxidation processes. *Environ. Sci. Technol.* 37 (5), 1016–1024.
- Jawad, A., Lu, X., Chen, Z., Yin, G., 2014. Degradation of chlorophenols by supported Co-Mg-Al layered double hydroxide with bicarbonate activated hydrogen peroxide. *J. Phys. Chem. A* 118 (43), 10028–10035.
- Jin, X., Jin, P., Hou, R., Yang, L., Wang, X.C., 2017. Enhanced WWTP effluent organic matter removal in hybrid ozonation-coagulation (HOC) process catalyzed by Al-based coagulant. *J. Hazard. Mater.* 327, 216–224.
- Jin, X., Shi, Y., Hou, R., Zhang, W., Jin, P., Wang, X., 2019a. Role of Al-based coagulants on a hybrid ozonation-coagulation (HOC) process for WWTP effluent organic matter and ibuprofen removal. *Environ. Sci. Water Res. Technol.* 5 (3), 599–608.
- Jin, X., Wang, Y., Zhang, W., Jin, P., Wang, X.C., Wen, L., 2019b. Mechanism of the hybrid ozonation-coagulation (HOC) process: comparison of preformed Al_{13} polymer and in situ formed Al species. *Chemosphere* 229, 262–272.
- Jin, X., Liu, Y., Wang, Y., Zhang, S., Zhang, W., Jin, P., Xu, L., Shi, X., Wang, X.C., Lv, S., 2020a. Towards a comparison between the hybrid ozonation-coagulation (HOC) process using Al- and Fe-based coagulants: performance and mechanism. *Chemosphere* 253, 126625.
- Jin, X., Xie, X., Liu, Y., Wang, Y., Wang, R., Jin, P., Yang, C., Shi, X., Wang, X.C., Xu, H., 2020b. The role of synergistic effects between ozone and coagulants (SOC) in the electro-hybrid ozonation-coagulation process. *Water Res.* 177, 115800.
- Kasprzyk-Hordern, B., Ziólek, M., Nawrocki, J., 2003. Catalytic ozonation and methods of enhancing molecular ozone reactions in water treatment. *Appl. Catal. B Environ.* 46 (4), 639–669.
- Khachatryan, L., Dellinger, B., 2011. Environmentally persistent free radicals (EPFRs)-2. Are free hydroxyl radicals generated in aqueous solutions? *Environ. Sci. Technol.* 45 (21), 9232–9239.
- Lee, Y., von Gunten, U., 2010. Oxidative transformation of micropollutants during municipal wastewater treatment: comparison of kinetic aspects of selective (chlorine, chlorine dioxide, ferrate^{VI}, and ozone) and non-selective oxidants (hydroxyl radical). *Water Res.* 44 (2), 555–566.
- Li, F., Zhang, L., Evans, D.G., Duan, X., 2004. Structure and surface chemistry of manganese-doped copper-based mixed metal oxides derived from layered double hydroxides. *Colloids Surf. A Physicochem. Eng. Asp.* 244 (1), 169–177.
- Li, X., Wang, Y., Yuan, S., Li, Z., Wang, B., Huang, J., Deng, S., Yu, G., 2014. Degradation of the anti-inflammatory drug ibuprofen by electro-peroxone process. *Water Res.* 63, 81–93.
- Lin, J.L., Huang, C., Dempsey, B., Hu, J.Y., 2014. Fate of hydrolyzed Al species in humic acid coagulation. *Water Res.* 56, 314–324.
- Liu, W., Ai, Z., Cao, M., Zhang, L., 2014. Ferrous ions promoted aerobic simazine degradation with $\text{Fe@Fe}_2\text{O}_3$ core-shell nanowires. *Appl. Catal. B Environ.* 150–151, 1–11.
- Magureanu, M., Piroi, D., Mandache, N.B., Părvulescu, V.I., Părvulescu, V., Cociararu, B., Cadigan, C., Richards, R., Daly, H., Hardacre, C., 2011. In situ study of ozone and hybrid plasma Ag-Al catalysts for the oxidation of toluene: evidence of the nature of the active sites. *Appl. Catal. B Environ.* 104 (1–2), 84–90.
- Meunier, L., Canonica, S., von Gunten, U., 2006. Implications of sequential use of UV and ozone for drinking water quality. *Water Res.* 40 (9), 1864–1876.

- Mu, Y., Ai, Z., Zhang, L., 2017. Phosphate shifted oxygen reduction pathway on Fe@Fe₂O₃ core-shell nanowires for enhanced reactive oxygen species generation and aerobic 4-chlorophenol degradation. *Environ. Sci. Technol.* 51 (14), 8101–8109.
- Nash, T., 1953. The colorimetric estimation of formaldehyde by means of the Hantzsch reaction. *Biochem. J.* 55 (3), 416–421.
- Nawrocki, J., 2013. Catalytic ozonation in water: controversies and questions. Discussion paper. *Appl. Catal. B Environ.* 142–143, 465–471.
- Nawrocki, J., Kasprzyk-Hordern, B., 2010. The efficiency and mechanisms of catalytic ozonation. *Appl. Catal. B Environ.* 99 (1), 27–42.
- Nöthe, T., Fahlenkamp, H., Sonntag, C.v., 2009. Ozonation of wastewater: rate of ozone consumption and hydroxyl radical yield. *Environ. Sci. Technol.* 43 (15), 5990–5995.
- Peng, F., Yin, R., Liao, Y., Xie, X., Sun, J., Xia, D., He, C., 2020. Kinetics and mechanisms of enhanced degradation of ibuprofen by piezo-catalytic activation of persulfate. *Chem. Eng. J.* 392, 123818.
- Rämö, J.H., Sarpolaa, A.T., Heikki Hellman, A., Leiviskä, T.A., Hietapelto, V.K., Jokela, J.T., Laitinen, R.S., 2008. Colloidal surfaces and oligomeric species generated by water treatment chemicals. *Chem. Spec. Bioavail.* 20 (1), 13–22.
- Rao, Y., Xue, D., Pan, H., Feng, J., Li, Y., 2016. Degradation of ibuprofen by a synergistic UV/Fe(III)/oxone process. *Chem. Eng. J.* 283, 65–75.
- Ren, Y., Dong, Q., Feng, J., Ma, J., Wen, Q., Zhang, M., 2012. Magnetic porous ferrosphalite NiFe₂O₄: a novel ozonation catalyst with strong catalytic property for degradation of di-n-butyl phthalate and convenient separation from water. *J. Colloid Interface Sci.* 382 (1), 90–96.
- Rubasinghe, G., Gurung, R., Rijal, H., Maldonado-Torres, S., Chan, A., Acharya, S., Rogelj, S., Piyasena, M., 2018. Abiotic degradation and environmental toxicity of ibuprofen: roles of mineral particles and solar radiation. *Water Res.* 131, 22–32.
- Ruggeri, G., Ghigo, G., Maurino, V., Minero, C., Vione, D., 2013. Photochemical transformation of ibuprofen into harmful 4-isobutylacetophenone: pathways, kinetics, and significance for surface waters. *Water Res.* 47 (16), 6109–6121.
- Rustad, J.R., Casey, W.H., 2006. A molecular dynamics investigation of hydrolytic polymerization in a metal-hydroxide gel. *J. Phys. Chem. B* 110 (14), 7107–7112.
- Saeid, S., Tolvanen, P., Kumar, N., Eränen, K., Peltonen, J., Peurla, M., Mikkola, J.-P., Franz, A., Salmi, T., 2018. Advanced oxidation process for the removal of ibuprofen from aqueous solution: a non-catalytic and catalytic ozonation study in a semi-batch reactor. *Appl. Catal. B Environ.* 230, 77–90.
- Sarpola, A., Hietapelto, V., Jalonen, J., Jokela, J., Laitinen, R.S., 2004. Identification of the hydrolysis products of AlCl₃·6H₂O by electrospray ionization mass spectrometry. *J. Mass Spectrom.* 39 (4), 423–430.
- Shu-xuan, D., Hui, X., Feng, X., Dong-sheng, W., Chang-qing, Y., Ru-yuan, J., Yan-jing, L., 2014. Effects of Al species on coagulation efficiency, residual Al and floc properties in surface water treatment. *Colloids Surf. A Physicochem. Eng. Asp.* 459, 14–21.
- von Sonntag, C., von Gunten, U., 2012. *Chemistry of Ozone in Water and Wastewater Treatment*. IWA Publishing.
- Staelin, J., Hoigne, J., 1982. Decomposition of ozone in water: rate of initiation by hydroxide ions and hydrogen peroxide. *Environ. Sci. Technol.* 16 (10), 676–681.
- Sun, Y., Chen, X., Lin, L., Xu, F., Zhang, X., 2021. Mechanisms and kinetics studies of the atmospheric oxidation of eugenol by hydroxyl radicals and ozone molecules. *Sci. Total Environ.* 770, 145203.
- Tang, H., Xiao, F., Wang, D., 2015. Speciation, stability, and coagulation mechanisms of hydroxyl aluminum clusters formed by PACl and alum: a critical review. *Adv. Colloid Interf. Sci.* 226, 78–85.
- Wang, J., Chen, H., 2020. Catalytic ozonation for water and wastewater treatment: recent advances and perspective. *Sci. Total Environ.* 704, 135249.
- Wang, L., Wang, F., Li, P., Zhang, L., 2013. Ferrous-tetrapolyphosphate complex induced dioxygen activation for toxic organic pollutants degradation. *Sep. Purif. Technol.* 120, 148–155.
- Wang, Y., Yang, W., Yin, X., Liu, Y., 2016. The role of Mn-doping for catalytic ozonation of phenol using Mn/γ-Al₂O₃ nanocatalyst: performance and mechanism. *J. Environ. Chem. Eng.* 4 (3), 3415–3425.
- Wang, D., Xu, H., Ma, J., Lu, X., Qi, J., Song, S., 2018. Strong promoted catalytic ozonation of atrazine at low temperature using tourmaline as catalyst: influencing factors, reaction mechanisms and pathways. *Chem. Eng. J.* 354, 113–125.
- Wang, T., Song, Y., Ding, H., Liu, Z., Baldwin, A., Wong, I., Li, H., Zhao, C., 2020. Insight into synergies between ozone and in-situ regenerated granular activated carbon particle electrodes in a three-dimensional electrochemical reactor for highly efficient nitrobenzene degradation. *Chem. Eng. J.* 394.
- Xiang, Y., Fang, J., Shang, C., 2016. Kinetics and pathways of ibuprofen degradation by the UV/chlorine advanced oxidation process. *Water Res.* 90, 301–308.
- Xiao, F., Zhang, B., Lee, C., 2008. Effects of low temperature on aluminum(III) hydrolysis: theoretical and experimental studies. *J. Environ. Sci.* 20 (8), 907–914.
- Xiong, Z., Lai, B., Yang, P., 2018. Insight into a highly efficient electrolysis-ozone process for N,N-dimethylacetamide degradation: quantitative analysis of the role of catalytic ozonation, fenton-like and peroxone reactions. *Water Res.* 140, 12–23.
- Xu, W., Gao, B., Yue, Q., Wang, Q., 2011. Effect of preformed and non-preformed Al₁₃ species on evolution of floc size, strength and fractal nature of humic acid flocs in coagulation process. *Sep. Purif. Technol.* 78 (1), 83–90.
- Yan, M., Wang, D., Ni, J., Qu, J., Chow, C.W.K., Liu, H., 2008. Mechanism of natural organic matter removal by polyaluminum chloride: effect of coagulant particle size and hydrolysis kinetics. *Water Res.* 42 (13), 3361–3370.
- Yang, L., Hu, C., Nie, Y., Qu, J., 2009. Catalytic ozonation of selected pharmaceuticals over mesoporous alumina-supported manganese oxide. *Environ. Sci. Technol.* 43 (7), 2525–2529.
- Yu, W.-Z., Gregory, J., Graham, N., 2016. Regrowth of broken hydroxide flocs: effect of added fluoride. *Environ. Sci. Technol.* 50 (4), 1828–1833.
- Zhang, T., Hou, P., Qiang, Z., Lu, X., Wang, Q., 2011. Reducing bromate formation with H (+)-form high silica zeolites during ozonation of bromide-containing water: effectiveness and mechanisms. *Chemosphere* 82 (4), 608–612.
- Zhang, Y., Ji, H., Liu, W., Wang, Z., Song, Z., Wang, Y., Liu, C., Xu, B., Qi, F., 2020. Synchronous degradation of aqueous benzotriazole and bromate reduction in catalytic ozonation: effect of matrix factor, degradation mechanism and application strategy in water treatment. *Sci. Total Environ.* 727, 138696.
- Zhang, B., Shan, C., Wang, S., Fang, Z., Pan, B., 2021a. Unveiling the transformation of dissolved organic matter during ozonation of municipal secondary effluent based on FT-ICR-MS and spectral analysis. *Water Res.* 188, 116484.
- Zhang, Y., Zhang, B.-T., Teng, Y., Zhao, J., Sun, X., 2021b. Heterogeneous activation of persulfate by carbon nanofiber supported Fe₃O₄/carbon composites for efficient ibuprofen degradation. *J. Hazard. Mater.* 401, 123428.
- Zhao, H., Liu, H., Qu, J., 2009a. Effect of pH on the aluminum salts hydrolysis during coagulation process: formation and decomposition of polymeric aluminum species. *J. Colloid Interface Sci.* 330 (1), 105–112.
- Zhao, L., Sun, Z., Ma, J., 2009b. Novel relationship between hydroxyl radical initiation and surface group of ceramic honeycomb supported metals for the catalytic ozonation of nitrobenzene in aqueous solution. *Environ. Sci. Technol.* 43 (11), 4157–4163.
- Zhao, H., Liu, H., Qu, J., 2011. Aluminum speciation of coagulants with low concentration: analysis by electrospray ionization mass spectrometry. *Colloids Surf. A Physicochem. Eng. Asp.* 379 (1), 43–50.
- Zhao, H., Dong, Y., Jiang, P., Wang, G., Zhang, J., Zhang, C., 2015. ZnAl₂O₄ as a novel high-surface-area ozonation catalyst: one-step green synthesis, catalytic performance and mechanism. *Chem. Eng. J.* 260, 623–630.